Available online at www.sciencedirect.com
ScienceDirect
Ceramics International 35 (2009) 2481–2491
CERAMICS INTERNATIONAL
www.elsevier.com/locate/ceramint

Preparation and mechanical characterization of dense and porous zirconia produced by gel casting with gelatin as a gelling agent

Jean-Marc Tulliani [a,*], Cecilia Bartuli [b], Edoardo Bemporad [c], Valentina Naglieri [a], Marco Sebastiani [c]

[a] *Materials Science and Chemical Engineering Dept., Politecnico di Torino, Corso Duca degli Abruzzi 24, 10129 Torino, Italy*
[b] *Chemical Engineering Materials Environment Dept., Sapienza University of Rome, via Eudossiana 18, 00184 Rome, Italy*
[c] *Mechanical and Industrial Engineering Dept., University of Roma 3, Via della Vasca Navale 79, 00146 Rome, Italy*

Received 2 January 2009; received in revised form 24 January 2009; accepted 13 February 2009
Available online 11 March 2009

Abstract

A modified gel casting procedure based on a natural gelatin for food industry and commercial polyethylene spheres as pore formers was successfully exploited to produce dense and porous ceramic bodies made of yttria stabilized tetragonal zirconia polycrystal (Y-TZP). Vickers and Knoop microhardness, elastic modulus and fracture toughness measurements on dense samples obtained by experimental investigation closely matched results found in the literature for similar materials. However, after a careful analysis of obtained results, no indentation size effect and a lower scattering of experimental data from low load indentations were observed, in comparison with literature.

Mechanical testing of porous samples (with reproducible values of porosity of about 40%) evidenced a high scattering of compressive strength values, suggesting that the uneven distribution of cavities in the material or the presence of defects from the agglomeration of pore forming agents could have a more direct influence on the mechanical properties of such materials than the absolute value of porosity.

Keywords: A. Suspensions; B. Porosity; C. Mechanical properties; D. ZrO_2

1. Introduction

The importance of porous ceramic materials is continuously increasing because of a variety of interesting applications, such as, molten metals filtration, high-temperature thermal insulation, support for catalytic reactions, filtration of particulates from diesel engine exhaust gases and of hot corrosive gases in various industrial processes, and scaffolds for bone substitution [1,2].

The characteristics of the pores influence the properties of the components, thus two crucial steps are involved in the production of cellular materials: first, the selection and set-up of a reliable forming method allowing a strict control of pore size, volume, distribution and morphology; second, the proper characterization procedures of the actual porosity features as well as of the mechanical/functional performance [1,2].

This paper mostly deals with the exploitation of a novel gel-casting process to develop dense and porous materials having controlled porosity characteristics.

Gel casting is a well-known, wet forming method based on the combination of ceramic processing and polymer chemistry. This process involves the dispersion of a ceramic powder into a monomer solution and casting of this suspension into a non-porous mould. Polymerization is then promoted and consequently ceramic particles are entrapped into the rigid and homogenous polymeric network [3]. After gel formation, gel-cast green materials can be easily de-molded and are then dried in controlled conditions.

The main advantages of this method are the high strength of the green bodies, allowing their machinability, the low amount of organic additives, avoiding a preliminary thermal treatment as in the injection molding process [4], and also its versatility which allowed to extend such process to a variety of ceramic materials.

Different monomers were exploited for gel casting, starting from acrylamide systems, now withdrawn due to their

* Corresponding author. Tel.: +39 011 5644700; fax: +39 011 5644699.
E-mail address: jeanmarc.tulliani@polito.it (J.-M. Tulliani).

0272-8842/$34.00
doi:10.1016/j.ceramint.2009.02.017

neurotoxicity [5], as well as alternative gelling agents, such as, for example, agar [6], agarose [6–8], carrageenan gums [6], egg white [9], gelatin [10–14] and polyvinyl alcohol [12].

Independently of the selected gelling agent, several problems related to porosity distribution control and mechanical strength tailoring as a function of process parameters still remain unsolved, and a comprehensive study is not yet present in literature.

In the present paper a natural gelatin, precisely a pig-derived product for food industry, was used. The natural gelling agents present the advantages of a polymerization just promoted by a temperature lowering, without the use of a catalyst and an initiator, as synthetic monomers do, and of a low environmental impact.

Hardness, elastic modulus, indentation size effect and fracture toughness of the bulk materials were evaluated by the use of a specifically developed mechanical characterization procedure, based on Vickers–Knoop microindentation testing and nanoindentation.

Gel-casting process was initially set-up for preparing dense components, and then modified to fabricate also porous ceramics, by combining it with foaming techniques, or replica methods, or even the addition of a sacrificial phase [1,15].

In this paper, a fugitive phase, made of commercial polyethylene spheres in a size range selected by sieving, was added to the ceramic suspension before gelling. The shape, size and size distribution of these spheres as well as their volume fraction with respect to the ceramic content into the slurry can allow a strict control of many porosity features of the final components. The feasibility of the modified process was demonstrated by developing porous components with a pore volume percentage of about 40 vol.%.

2. Materials and methods

2.1. Sample preparation and characterization of the green bodies

Commercial stabilized zirconia with 3 mol% of yttria (yttria tetragonal zirconia polycrystal, Y-TZP, grade TZ-3Y supplied by Tosoh Co., Japan) was used for preparation of ceramic suspensions having a solid loading of 60 wt% and dispersed into water at natural pH by ultrasonication for 10 min [13]. Particle size distribution was determined by means of a laser granulometer (Fristch analysette 22) in ethanol after 10 min of ultrasonication.

A pig skin-derived gelatin produced by Italgelatine (Italy) was chosen as gelling agent: its melting point is 32.5 °C and its viscosity in aqueous solution (6.67 wt%) at 60 °C is 42.5 mPa s with a related pH of 5.08. This gelatin calcined up to 550 °C for 18 h yielded a limited amount of residual ashes (0.2 wt% of the starting mass), as confirmed by the thermogravimetric analysis [14]. For suspensions preparation, the gelatin was dissolved into deionized water at 60 °C and this solution was then added to the ceramic suspensions at the same temperature under stirring, so that an amount of gelling agent of 3 wt%, with respect to the final water content, was reached. Several tests were carried out to determine the optimal gelatin amount: on one hand, a content less than 1 wt% did not allow the formation of a continuous network and green bodies could not be handled, on the other hand an excess of 4 wt% resulted in too viscous suspensions for casting [10].

A polyethylene (PE) powder, supplied by Clariant Italia SpA, having a density at 23 °C of about 0.92–0.94 g/cm^3 was used as fugitive phase. Its thermal decomposition is almost completed after calcination at 550 °C [14].

PE powder was made of almost spherical particles, but irregular structures were also present. Polyethylene spheres were firstly sieved in the range 125–300 μm, before dispersion into ceramic suspensions. It must also be noted that during sieving few smaller particles remained adherent to the larger ones, so that a limited fraction of pores smaller than those expected from the sieved range could be observed in the final materials and irregular pore geometry can be yielded (Fig. 1) [13].

In a first step, to set-up the procedure, dense components were produced by adding ceramic powders to deionized water to prepare ceramic suspensions having 60 wt% solid content.

Gelatin has a strong tendency to favor foam formation during preparation [10,11], therefore, a de-airing step was required to remove air bubbles entrapped into the ceramic suspensions: casting of the suspensions was carried out under vacuum (at about 10^{-2} Pa), by pouring into non-porous Plexiglas moulds at 60 °C and then cooling down to room temperature for promoting gelation. Cylindrical molds having different dimensions (internal diameter from 12 up to 18 mm and height in the range 30–55 mm) were used. In a first moment, the cast samples were slowly dried at room temperature under a controlled humid atmosphere and then, after de-molding, in static air.

To fabricate porous ceramics, PE spheres were added to the powder suspensions after a preliminary dispersion in water, in suitable amounts to obtain zirconia bodies having about 40 vol.% porosity. The ceramic content of the slurries was the same adopted for the dense materials.

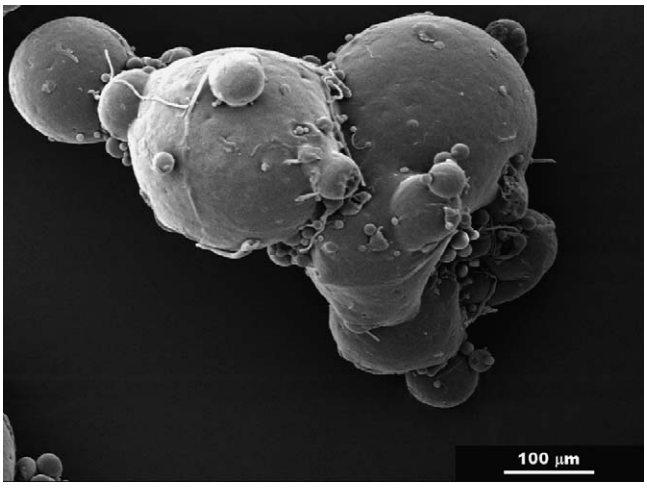

Fig. 1. SEM micrograph of the PE spheres used as a pore formers.

Dense gel-cast zirconia ceramics were sintered at 1550 °C (heating rate of 5 °C/min, soaking time of 1 h at the maximum temperature and cooling down to room temperature at 10 °C/min). The sintering cycle was set-up on the basis of dilatometric studies performed on gel-cast bars [13].

Another difference between dense and porous samples consisted in the modification of the overall thermal cycle during heating up to 600 °C: various intermediate steps, on the basis of the TGA results described on a previous work [14], have to be introduced to control the thermal decomposition of the polyethylene spheres, without collapsing of the structure.

The as-received powders were characterized by TEM microscopy techniques (TEM-FEI CM120, LaB_6, double tilt, nanoprobe, analytical set-up): samples were prepared by direct immersion of the TEM sample holder grid (formvar film on 3 mm copper grid) in a solid suspension into ethanol and ultrasonic bath of the ceramic powder. Knoop microhardness (Mitutoyo HM-124 microhardness tester, applied load 0.25 N, other test parameters in accordance with ASTM E384 standard) was firstly measured onto two green gel cast samples: one completely dried under air and another one, in a controlled humidity chamber, in order to check the influence of drying conditions onto the mechanical properties of the samples. These samples were previously dry cut with a diamond saw at 200 rpm and with a speed rate of 1.2 mm/min in order to obtain a flat surface free from artifacts.

2.2. Mechanical characterization of dense samples

Knoop indentation tests were also used on sintered ceramics to estimate the elastic modulus, by the use of the widely adopted model developed by Marshall et al. [16]:

$$\frac{H_K}{E} = \frac{0.14 - (b/d)}{0.45} \tag{1}$$

where b and d are the lengths of the shorter and longer Knoop diagonals, respectively.

Hardness and indentation size effect of dense samples were investigated by Vickers indentation testing, applied loads ranging from 0.1 to 20 N (ASTM E384 standard). Six indentations were performed for each load.

The indentation size effect (ISE) Meyer's law [17] was finally adopted to describe the relation between load and size of indentation:

$$P = kd^n \tag{2}$$

where P is the applied load, d is the indentation size, k and n are the constants.

Eq. (2) can be rewritten as a function of Vickers hardness:

$$H_V = H_{V0}d^{n-2} \tag{3}$$

Coefficient n is known as Meyer's or hardening index, generally lower than 2.0 for pyramidal indenters [17,18], while H_{V0} is a constant. If n is equal to 2, there is no ISE in the analyzed sample.

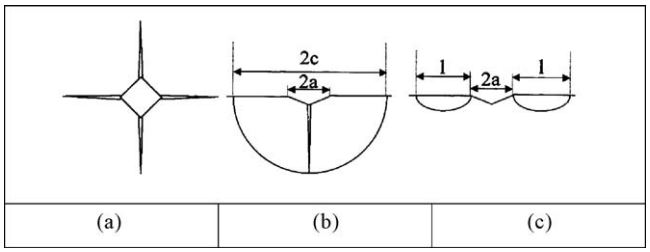

Fig. 2. (a) Crack generation after Vickers indentation; (b) radial-median (Penny-like) crack geometry (section view); (c) Palmqvist crack geometry (section view).

Vickers hardness testing was also adopted for fracture toughness evaluation of the bulk zirconia samples: during sharp indentation of brittle materials, radial cracks can be generated during unloading due to the residual crack opening force given by the plastic deformed zone under the indenter [19–27].

Under sharp indenters, two distinct types of crack are found in planes perpendicular to the direction of indentation (Fig. 2): (1) penny-like (or radial-median) crack type, where the crack is generated all under the indent and (2) Palmqvist crack type, where a crack is developed only at the corners of the indent. Usually low toughness materials show radial-median crack type, while high toughness materials show Palmqvist crack type; it is also very common that both behavior are observed for the same material as a function of the applied load; in this case a transition zone between crack type (1) and type (2) can also be identified [27].

Although several empirical models can be found in literature [21–25], they can be classified depending on the hypothesis on crack geometry, and two basic equations can be written:

$$K_{ICM} = \alpha\left(\frac{E}{H}\right)^q \frac{P}{c^{3/2}}, \text{ for radial-median cracks} \tag{4}$$

$$K_{ICM} = \beta\left(\frac{E}{H}\right)^r \frac{P}{al^{1/2}}, \text{ for Palmqvist cracks} \tag{5}$$

where α and β are the empirical constants, q and r are the exponents which take different values depending on the considered model [21–25], P is the applied load, a is the half diagonal of the indent, c is the crack length from the centre of the indent, l is the crack length from the corner of the indent (see Fig. 2).

Other models exist [26,27] which do not have any preliminary hypothesis on crack geometry and are derived by direct fitting of experimental data coming from a set of indentations obtained in a wide applied load range which combines both radial-median and Palmqvist crack regimes [26,27].

However, a criterion is available to discriminate between Palmqvist and radial-median crack, based on the measured c/a ratio (Fig. 2), if:

$$\begin{aligned} &\frac{c}{a} \le 2.5 \quad \text{Palmqvist} \\ &\frac{c}{a} \ge 2.5 \quad \text{Half-Penny} \end{aligned} \tag{6}$$

Table 1
Adopted models for fracture toughness evaluation from standard Vickers indentation (applied load in N, crack length in mm).

Model	Ref.	Hypothesis on crack geometry
Anstis et al.	[21]	Radial-median
Lawn et al.	[22]	Radial-median
Laugier	[23]	Radial-median
Niihara et al.	[24]	Palmqvist
Laugier et al.	[25]	Palmqvist
Lankford	[26]	No hypothesis

In the present paper, six models based on different assumptions on crack shape have been considered for fracture toughness evaluation of the produced dense zirconia samples (as summarized in Table 1).

For this application, Vickers hardness testing has been performed with an applied load of 20 N, while crack length and crack geometry were analyzed by Digital Optical Microscopy; Vickers hardness number H_V (ASTM E384) was used for all models, correcting the empirical constants when necessary.

Nanoindentation testing [28,29] was performed by means of a Berkovich diamond indenter, using an MTS G200 Nano Indenter, in a continuous stiffness measurement mode (CSM) under a constant strain rate of 0.05 s^{-1} and a maximum load of 650 mN (other test and fitting parameters were chosen according to ISO 14577-1-2 standards).

In case of the adopted CSM method, the contact stiffness is dynamically measured during indentation, as the indenter is driven in during loading, and continuous hardness/depth and modulus/depth curves are then obtained (Fig. 3). Elastic modulus and hardness profiles are then accessible without direct imaging of the indentation [28]. The hardness H is derived by Eq. (7):

$$H = \frac{P_{\max}}{A} \tag{7}$$

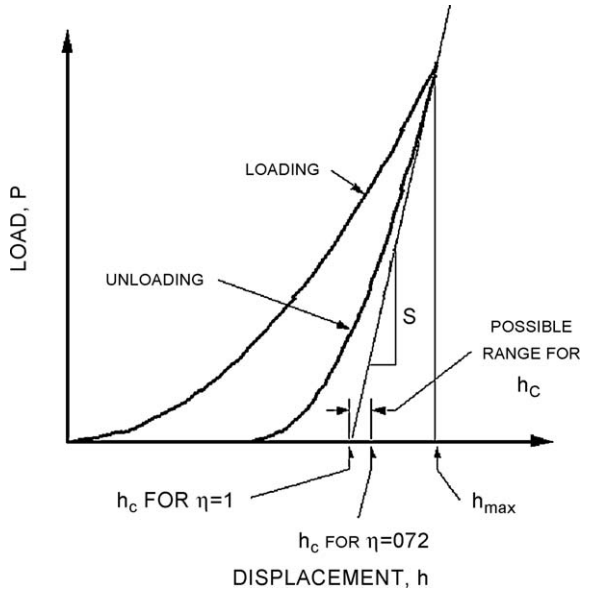

Fig. 3. Schematic of typical load-displacement data defining key experimental quantities.

where A is the indenter projected contact area, which is given as a polynomial function of the contact depth h_c, for a Berkovich indenter [28]:

$$A = a_0 h_c^2 + a_1 h_c + a_2 h_c^{1/4} + a_3 h_c^{1/8} + \cdots \tag{8}$$

Being the contact depth defined as follows [28]:

$$h_c = \frac{h - \eta P}{S} \tag{9}$$

The coefficient η can range between 0.72 and 1 (Fig. 3); a value of 0.75 is usually adopted for Berkovich indenter [28].

The contact area expressed in Eq. (8) is finally evaluated by calibration on certified fused silica reference sample, performed before and after each series of tests on dense zirconia.

The reduced elastic modulus is calculated by the following equation [29–31]:

$$E_r = \frac{\sqrt{\pi}}{2\beta}\frac{S}{\sqrt{A}} \tag{10}$$

$S = dP/dh$ is the elastic contact stiffness which is evaluated, after fitting the upper portion (usually 50%) of the unloading curve to a power-law relation (Oliver–Pharr method [28]), as the slope of the unloading curve at maximum load $P_{\max}$ (Fig. 3).

β is a numerical factor equals to 1.034 for a Berkovich indenter, related to a lack of symmetry of the indenter [30]. As recently reviewed by Oliver and Pharr [29], values in the range of $1.0226 \leq \beta \leq 1.085$ can be found in literature; in the present work a value of 1.000 was adopted, as suggested by the ISO 14577-1-2 standard. However, recent studies [29] have underlined that further corrections factors should be adopted.

The elastic modulus of the tested samples can then be estimated by Eq. (11):

$$\frac{1}{E_r} = \frac{(1-\upsilon)^2}{E} + \frac{(1-\upsilon_i)^2}{E_i} \tag{11}$$

where E_i and υ_i are, respectively, the Young's modulus and the Poisson ratio of the indenter.

In all cases, the cross-sections of the samples were polished before indentation by the use of diamond lapping films in 15, 6, 3 and 1 μm grades, 1 min each.

Finally, mechanical characterization of porous materials was carried out performing uniaxial compressive tests (Zwick/Roell Z010 electromechanical testing machine) on cylindrical samples, according to ASTM 1424-99 indications. Samples with proper geometry (aspect ratio length/diameter ≅ 1.5, maximum parallelism between plane surfaces), were produced by a precise sectioning machine from as-densified ceramic specimens. Ten samples were tested, with relative densities comprised between 59.3% and 63.0%.

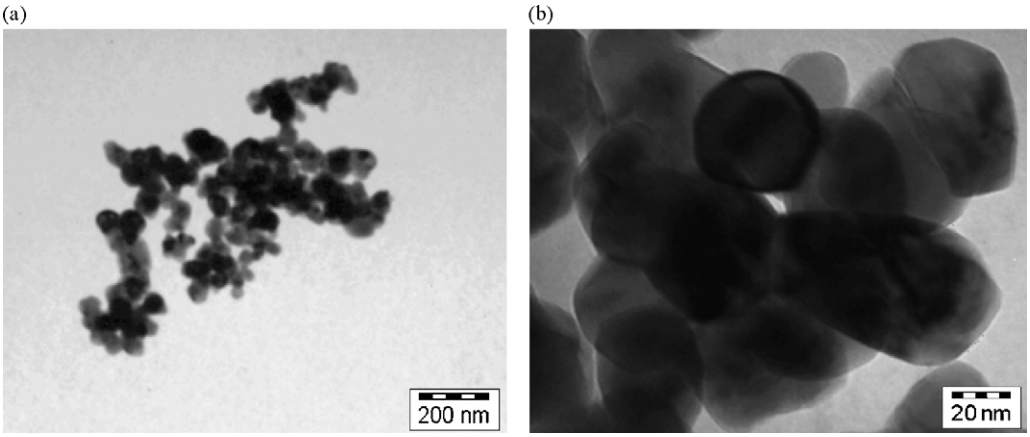

Fig. 4. Bright field TEM micrographs of zirconia powder TZ-3Y: (a) 40,000× and (b) 380,000×.

3. Results

3.1. Powders characterization

After 10 min of ultrasonication, the mean diameter of the zirconia powder was about 0.6 μm and the diameters corresponding to 10% and 90% of the particle size distributions were, respectively, 0.33 and 1 μm.

TEM observations revealed that powder grains were almost regular and agglomerated into clusters up to 1 μm in diameter (Fig. 4). Image analysis on 50 grains showed that mean crystallite size was about 24 nm and the standard deviation was 8.5 nm.

3.2. Dense sample characterization

Knoop microhardness was firstly measured onto two types of green gel cast samples: one completely dried under air and another one under a controlled atmosphere, to evidence possible gradients of hardness from the bulk of the sample to the surface. An applied load of 0.25 N gave the best compromise: lower values resulted in large reading errors of indents dimensions, while higher loads led to sample breaking. Knoop microindenter was chosen because of its asymmetry and low penetration depth which allowed a more local analysis of the hardness.

The hardness was measured along a line perpendicular to the casting direction (Fig. 5).

For both samples, hardness values are rather constant, even if a transition zone is present, in which hardness continuously decreases from the outer surface to the bulk of the sample. Such transition zones are about 600 and 350 μm thick, respectively for the sample only dried under air and for the one dried in a controlled atmosphere (Fig. 6).

After firing at 1550 °C for 1 h, the relative density of a dense cylinder reached 97% of theoretical density. On this sample, a 1 mm slice was cut and mirror polished, prior to thermal etching (18 min @ 1500 °C, with an heating ramp of 5 °C/min) and SEM observations (Fig. 7).

Knoop microhardness (10 N applied load) was determined on another sintered sample at 1550 °C for 1 h, having a geometrical density of 95.5%. The average values for hardness and elastic modulus (Marshall model) are reported in Table 2.

Results of Vickers hardness testing are also presented in Table 3, while the ISE curve is reported in Fig. 8: in this case, H_{V0} and n from Eq. (3) were equal to 15.91 GPa and 1.89,

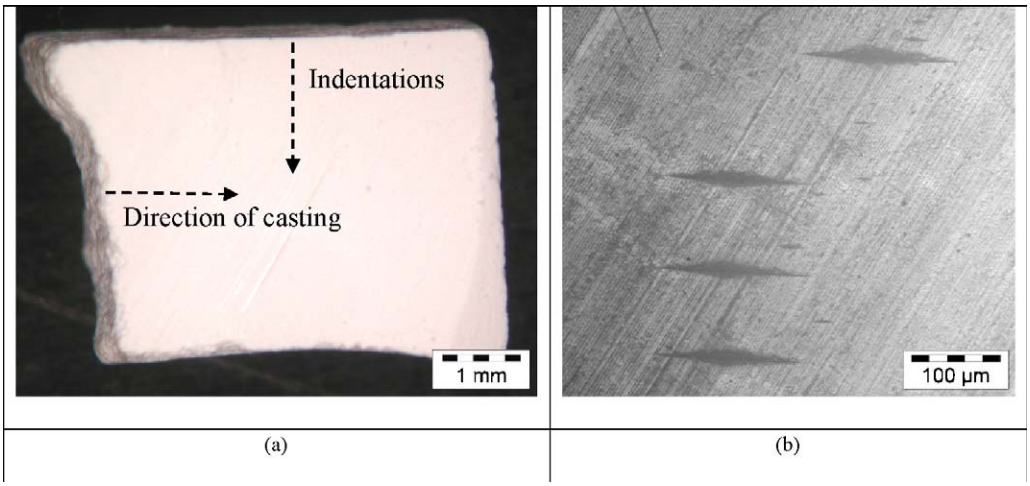

Fig. 5. Cross-section of gel cast TZ-3Y sample (a) and (b) some of the Knoop microindentations.

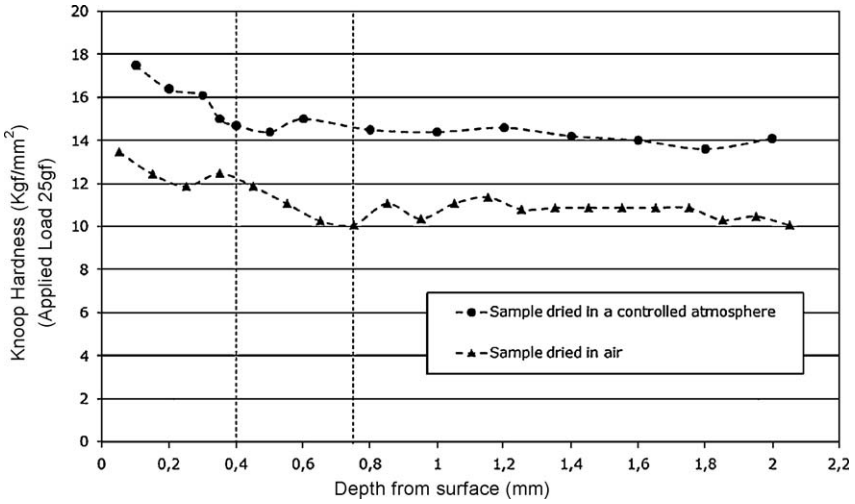

Fig. 6. Knoop microhardness for the gel cast sample dried in air and in a controlled atmosphere. Dashed lines report the extension of the skin effect detected in both cases.

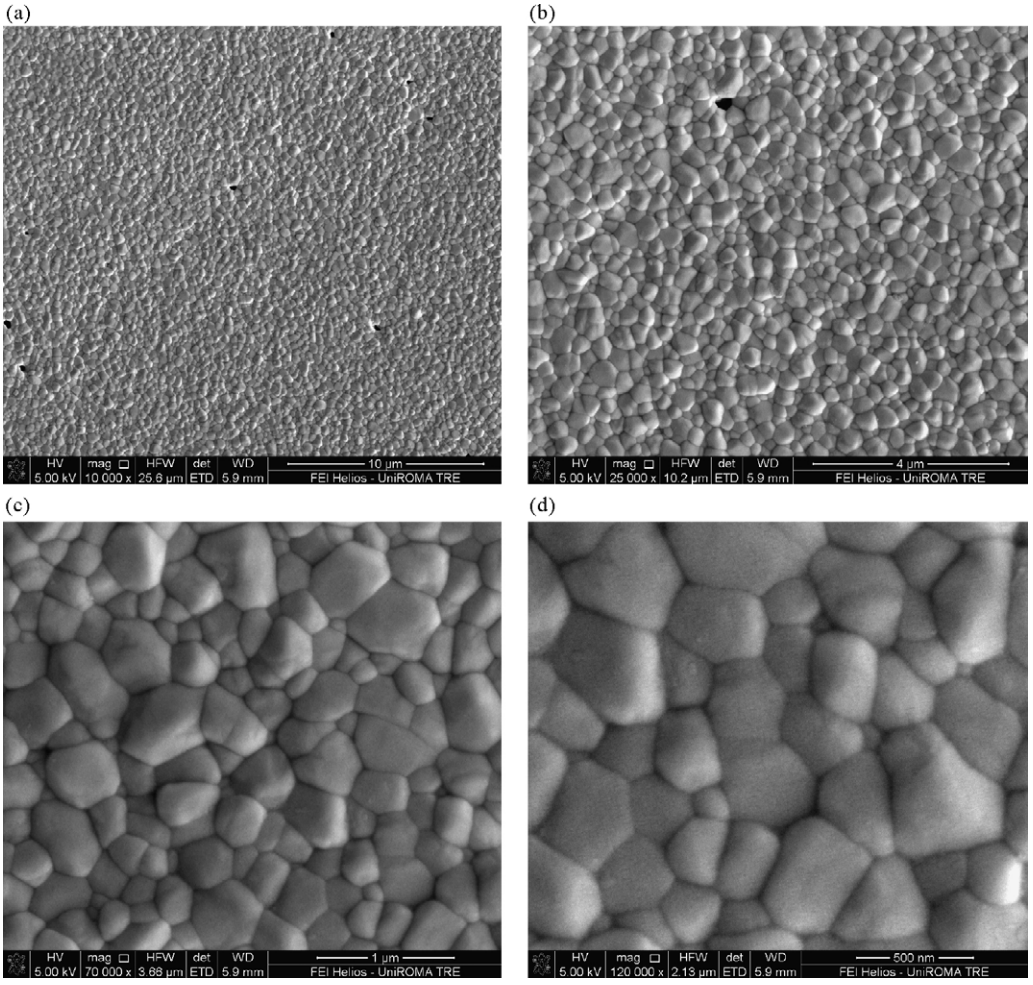

Fig. 7. SEM micrographs of the dense zirconia sample (bar = 10 μm (a), 4 μm (b); 1 μm (c) and 0.5 μm (d)).

respectively, so a significant ISE is predicted by Vickers indentation testing.

Fracture toughness results of the analyzed samples are reported in Fig. 9: it can be observed that different values are obtained depending on the hypothesis on crack geometry: in particular models based on radial-median crack geometry give an average value of 5.5 MPa $m^{0.5}$ while models based on Palmqvist crack geometry give an average value of

Table 2
Mean values of Knoop microhardness and Young's modulus on a 95.5% dense sample.

	Average value	Standard deviation
H_K (10 N) (GPa)	9.89	0.34
H/E	0.046	0.002
E (GPa)	212.85	14.64

Table 3
Vickers microhardness on a 95.5% dense sample.

Load (N)	H_V (GPa) (average of six values and standard deviation)	Mean indentation size d_m (μm)	Estimated indentation depth (1/7 × d_m) (μm)
10	11.22 ± 0.54	40.81 ± 1.05	5.83 ± 0.15
5	11.01 ± 0.15	29.02 ± 0.20	4.15 ± 0.03
3	10.61 ± 0.18	22.90 ± 0.19	3.27 ± 0.03
2	11.64 ± 0.76	17.87 ± 0.59	2.55 ± 0.08
1	11.73 ± 1.10	12.60 ± 0.60	1.80 ± 0.09
0.5	11.43 ± 0.69	9.02 ± 0.26	1.29 ± 0.04
0.25	13.68 ± 0.21	5.82 ± 0.05	0.83 ± 0.01
0.10	14.30 ± 2.21	3.63 ± 0.28	0.52 ± 0.04

8.9 MPa $m^{0.5}$. On the other hand, the Lankford model (no hypothesis on crack geometry [26]) gave a fracture toughness of 10.1 MPa $m^{0.5}$.

Results of nanoindentation testing are presented in Figs. 10–13 and Table 4: no significant variation of the elastic modulus and of the hardness with depth were detected, being values of elastic modulus and hardness in good accordance to literature.

3.3. Porous samples characterization

On a mirror polished section of a porous sample (having a geometrical density of 59.5%, five optical images (50× magnification) were recorded, then binarized and the porosity features were analyzed (Figs. 14 and 15 and Table 5). The overall investigated area was about 8.9 mm^2 and porosity represented 40.1% of it.

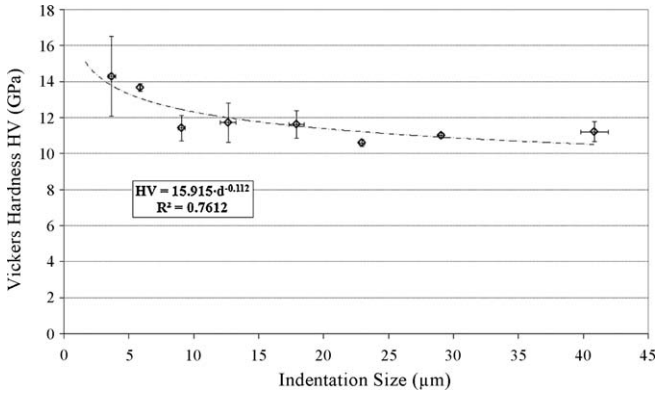

Fig. 8. Relationship between indentation test load and indentation size.

Uniaxial compressive tests were then performed onto porous cylinders (Table 6).

4. Discussion

4.1. Dense samples

Dense zirconia samples having up to 97% of the theoretical density, with submicronic grains, were produced by an improved gel-casting process based on gelatin.

It is shown that by the combined use of Vickers–Knoop microindentation and nanoindentation techniques, and a proper application of the models available in literature, reproducible data can be obtained on elastic modulus, hardness and fracture toughness of samples; indentation testing is then confirmed to be an effective micro-probe for the investigation of mechanical properties of dense ceramic bodies.

In the case of green samples, Knoop indentation testing was successfully adopted for the indirect evaluation of sample density, and a clear difference between different drying procedure was observed: the sample dried under controlled conditions showed higher values of hardness, respect to the one dried under air, in the bulk, as well as, within the transition

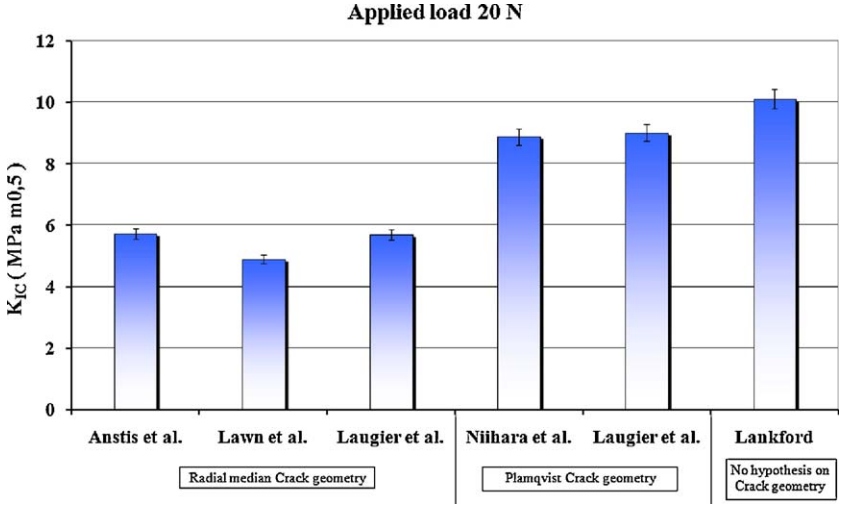

Fig. 9. Calculated K_{IC} values according to literature models.

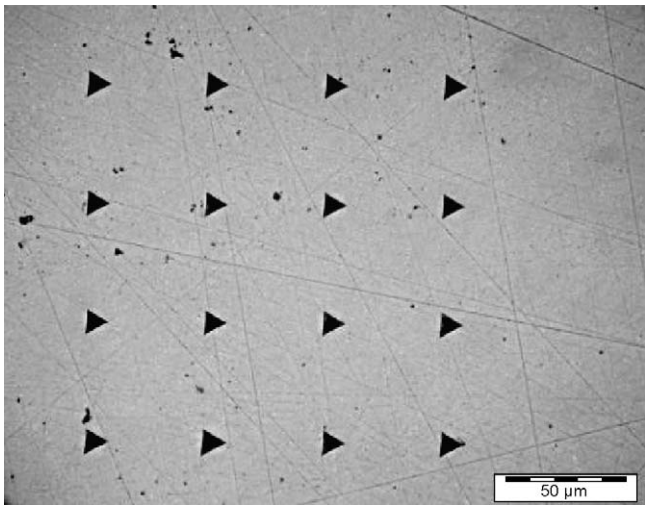

Fig. 10. Berkovich nanoindentations on a dense zirconia sample.

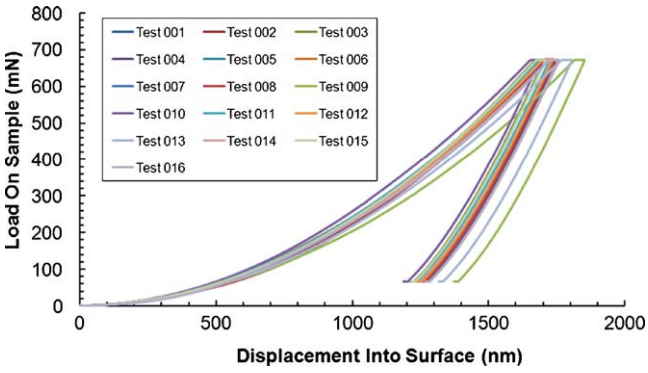

Fig. 11. Load–depth curves after indentations of the dense sample.

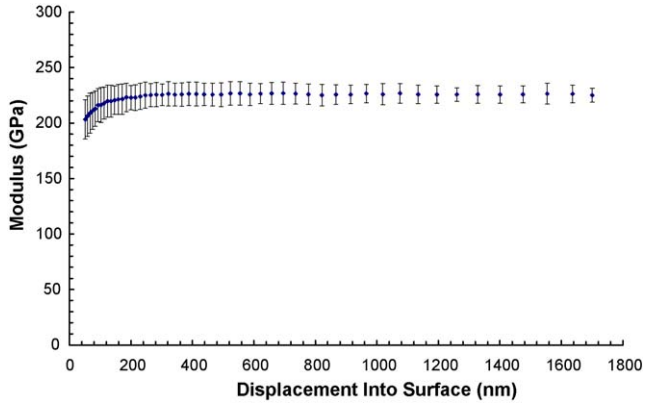

Fig. 12. Elastic modulus as a function of the penetration depth, assuming a Poisson ratio of 0.3 (statistical processing of the 16 indentations).

zone, this demonstrates the higher compaction grade of the powder in the green sample.

Previous works [32] have already demonstrated that a correlation exists between scratch hardness and density distribution of green ceramic bodies, and a measurement of density gradients is possible with a spatial resolution of about 100 μm; as the compaction grade of the grains is correlated to the locally applied pressure, a difference in the hardness can be

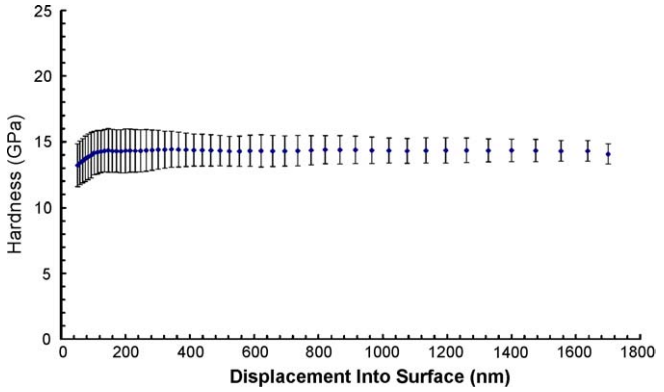

Fig. 13. Hardness as a function of the penetration depth (statistical processing of the 16 indentations).

Table 4
Mean Knoop hardness and Young's modulus for a 95.5% dense zirconia.

Average Knoop hardness (GPa)	Average Young's modulus (GPa)	Depth range considered for averaging (nm)
14.32 ± 1.02	226.11 ± 8.39	400–1500

seen as a difference in density, thus to the presence or not of porosities. In addition, scratch hardness is also found to be a function of particle shape and size, deformation property of the binder, agglomerates size, void sizes and the extent of bridging that may occur inside the compact [32]. In the present work, the gradient of density is due to capillary forces during drying conditions of the samples.

In this case, the use of Knoop hardness instead of scratch testing can give a less invasive way for density indirect evaluation, maintaining a similar, or even better, spatial resolution (see Fig. 5b).

In the case of dense zirconia samples, the measured elastic modulus corresponds to the elastic modulus of dense 3Y-TZP ceramics, and confirms the rather high density of the samples [33,34].

It is noteworthy that elastic modulus values obtained by Knoop indentation and nanoindentation are very similar: this confirms how effective, cheap and quick can be the use of the Marshall model [16] for the evaluation of the elastic behavior of ceramics.

On the other hand, different hardness values were obtained depending on the adopted technique and a deeper discussion is necessary.

First of all, it has to be reminded that different hardness definitions and contact area evaluation procedures are used depending on the considered technique, which often lead to non comparable values and a different measured ISE behavior depending on the considered indenter, mostly as a consequence of indenter tip blunting, which is much more pronounced in case of Vickers indenters compared to Berkovich.

As clearly visible from Fig. 8, obtained Vickers hardness values are rather constant for an indentation size higher than 10 μm (i.e. for applied load higher than 50 gf and penetration depth higher than 1.4 μm); as the applied load decreases, a

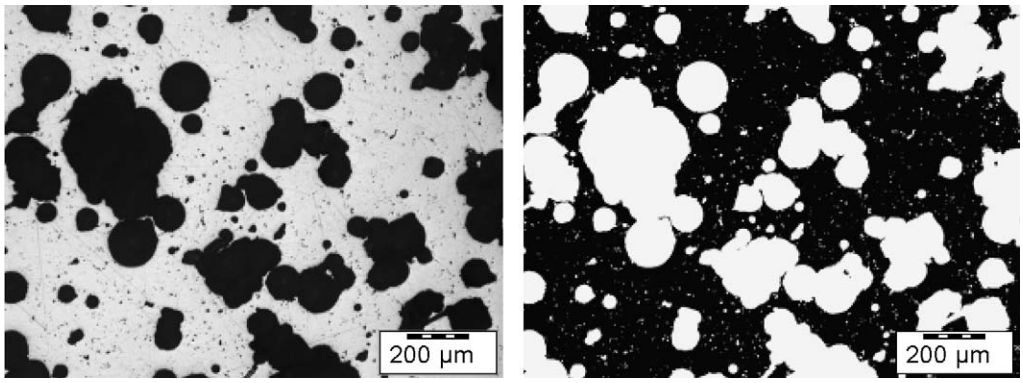

Fig. 14. Optical image (a) and (b) binarized image of a 59.5% dense cylinder (sample no. 9 in Table 6).

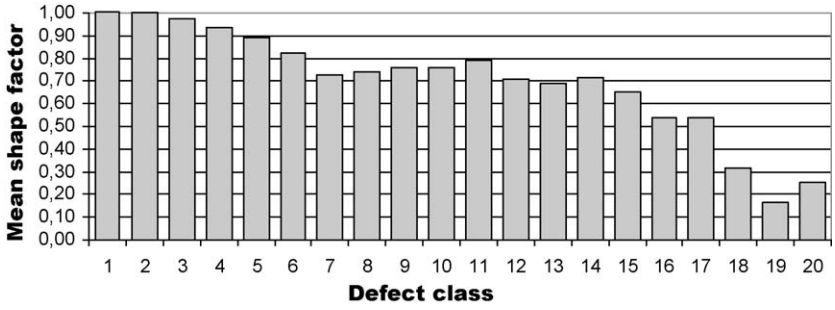

Fig. 15. Shape factor distribution per class.

sudden increase of microhardness values is observed. Considering that a Vickers indenter is usually characterized by a blunted tip with a tip radius of 500–1000 nm [35], this behavior is very likely due to tip rounding effects [36], more than a real indentation size effect, and an overestimation of the hardness values for low applied load is very likely to happen [36].

The Meyer index obtained by Vickers indentation is therefore in this case mainly due to tip blunting: furthermore, as a pure empirical equation, Meyer's law cannot provide any knowledge of the origin of ISE [37], which for ceramic materials has been identified to be due not only to different microstructural sources (such as grain size, elastic/plastic transition, soft surface layers and fracture), but also to artifacts due to tip blunting.

In order to assess this hypothesis, nanoindentation testing (Figs. 10–13) was performed adopting a new Berkovich indenter tip, with a nominal tip radius of 20 nm: in this case, no

Table 5
Results of image analysis on porous zirconia cylinders.

Defect	Area interval (μm^2)		Number of defects	Mean area (μm^2)	Mean shape factor
	Min	max			
1	0.50	0.95	638	253.182	1.080
2	0.95	1.82	781	531.495	1.008
3	1.82	3.46	1393	1708.907	0.975
4	3.46	6.60	1392	3147.005	0.938
5	6.60	12.57	1161	4775.955	0.893
6	12.57	23.97	717	5375.805	0.822
7	23.97	45.68	360	4986.143	0.730
8	45.68	87.06	153	3935.320	0.740
9	87.06	165.92	79	3855.590	0.760
10	165.92	316.23	54	5018.668	0.760
11	316.23	602.70	23	3772.790	0.790
12	602.70	1148.70	24	7894.977	0.710
13	1148.70	2189.32	18	11,070.305	0.692
14	2189.32	4172.65	21	23,312.674	0.717
15	4172.65	79,52.71	12	24,382.150	0.650
16	7952.71	15,157.17	20	75,808.250	0.535
17	15,157.17	28,888.23	13	96,628.477	0.540
18	28,888.23	55,058.45	18	227,122.313	0.317
19	55,058.45	104,936.60	7	160,792.500	0.162
20	104,936.60	200,000.00	5	230,930.359	0.252

Table 6
Compressive strength of porous cylinders.

Sample	Relative density (%)	Compressive strength (MPa)
1	63.00	193.9
2	59.30	235.7
3	59.90	236.2
4	60.40	177.7
5	63.8	220.5
6	60.93	178.1
7	62.70	157.6
8	62.56	186.1
9	59.49	224.1
10	64.83	295.2
Average (± St. Dev.)	61.68 ± 1.95	210.51 ± 40.21

significant variation of the elastic modulus and of the hardness with depth were detected, thus confirming the absence of indentation size effects, as previously observed with Vickers microhardness measurements.

This results suggest how the analysis of very low load Vickers hardness data can often lead to incorrect results due to tip blunting effect, and how the use of very sharp indenters (and a proper tip calibration) is necessary for a correct evaluation of size effects in ceramics.

In the case of fracture toughness evaluation from Vickers indentation testing, consistent results with low scattering of experimental data are obtained for each class of models, although significant differences between different classes of models still remains.

A selection of the correct toughness value can be performed considering that the average value of the *c/a* ratio was 1.28, this suggests that a Palmqvist cracking mode occurs in this case and that only the models based on this hypothesis should be considered: the proper toughness value of the samples can be therefore taken as 8.9 MPa $m^{0.5}$, according to the presented Palmqvist-based models.

These results are in agreement with what observed in the literature for Y-TZP ceramics with a toughness of 8 MPa $m^{0.5}$, which show Palmqvist cracks under indentation loads less than 625 N [18].

Strong care must be also taken in the correct choice of the hardness value to be used in Eq. (6): it has been underlined in literature [38] how the existence of the indentation size effect [17] in hardness testing makes it insufficient to quote a single hardness number when hardness is used in material characterization, and suggest to adopt a comparable hardness index for fracture toughness evaluation, that is the hardness value measured at relatively high load, and without the presence of cracks, to make it nearly load-independent.

As discussed before, no ISE during Vickers indentation was observed for the load range between 0.5 and 10 N: the adopted hardness parameter for toughness evaluation was therefore calculated as the average Vickers number over this load range.

4.2. Porous samples

A micro- and a macroporosity were clearly identified in the samples (Table 5): smaller defects belonging to the classes 1–5 (up to 12.6 μm^2) correspond to roughly circular porosities (with a shape factor of ca. 0.89), while macroporosities (up to 200,000 mm^2) have a smaller shape factor (0.252) and are thus less regular objects. These objects are probably due to a non-optimal PE spheres dispersion or to non-perfectly spherical pore agents within the suspension (Fig. 1).

Concerning compressive tests, though the density values of the samples were rather close (Table 6), the compressive strength differ significantly within the samples, without an evident relationship. The presence of huge defects as the ones evidenced by image analysis (Table 5) is probably responsible for the results scattering. These defects may have been caused because of the PE irregular structures sometimes present (Fig. 1). More regular polymethyl methacrylate (PMMA) powders were used in Ref. [39] and led to more homogeneous microstructures with interesting mechanical properties. In this study, the choice of polyethylene powder was dictated by the lower environmental impact during thermal decomposition.

5. Conclusions

Dense and porous ceramic bodies based on yttria tetragonal zirconia polycrystal were successfully produced by a gel-casting process based on a natural gelatin for food industry and commercial polyethylene spheres used as pore formers. As already pointed out by other authors [11], de-airing step is of crucial importance, as well as the long time for gelation and above all for drying in controlled conditions. Dense samples reached 96–97% of theoretical density with a fine microstructure, thus Vickers and Knoop hardness, as well as, elastic modulus and fracture toughness measurements on dense samples gave results comparable to data found in literature.

The specifically developed procedure based on indentation testing allowed a better control of the mechanical properties of dense sample, enhancing the statistical validity of obtained data and giving the correct correlation between process parameters and mechanical properties of samples. In particular, artifacts coming from tip blunting during Vickers indentation were highlighted and a better evaluation of size effects during indentation is given. Furthermore, the correct use of the models for fracture toughness evaluation also allowed to obtain reproducible results.

The tested porous samples presented closed porosities values (around 40%) but the irregular shape of the polyethylene spheres and the presence of non-dispersed spheres aggregates were responsible for compressive strengths scattering. A more regular polymer powder would have been better as a pore former agent.

Acknowledgements

The authors wish to thank the Italian Inter-University National Consortium on Material Science and Technology (INSTM) to have supported this research in the framework of the Prisma Project 2005 ‘‘Development of new cellular materials by gel-casting technique: optimization of production process and functional simulation of the microstructure’’.

References

[1] A.R. Studart, U.T. Gonzenbach, E. Tervoort, L.J. Gauckler, Processing routes to macroporous ceramics: a review, Journal of the American Ceramic Society 89 (6) (2006) 1771–1789.
[2] P. Colombo, Conventional and novel processing methods for cellular ceramics, Philosophical Transactions of the Royal Society A 364 (2006) 109–124.
[3] O.O. Omatete, M.A. Janney, R.A. Strehlow, A new ceramic forming process, American Ceramic Society Bulletin 70 (10) (1991) 1641–1649.
[4] A.C. Young, O.O. Omatete, M.A. Janney, P.A. Menchhofer, Gelcasting of alumina, Journal of the American Ceramic Society 74 (1991) 612–618.
[5] M.A. Janney, O.O. Omatete, C.A. Walls, S.D. Nunn, R.J. Ogle, G. Wastmoreland, Development of low-toxicity gelcasting systems, Journal of the American Ceramic Society 81 (3) (1998) 581–591.

[6] A.J. Millán, R. Moreno, M.I. Nieto, Thermogelling polysaccharides for aqueous gelcasting. Part I. A comparative study of gelling additives, Journal of the European Ceramic Society 22 (2002) 2223–2230.
[7] I. Santacruz, M.I. Nieto, R. Moreno, Alumina bodies with near-to-theoretical density by aqueous gelcasting using concentrated agarose solutions, Ceramics International 31 (2005) 439–445.
[8] E. Adolfsson, Gelcasting of zirconia using agarose, Journal of the American Ceramic Society 89 (6) (2006) 1897–1902.
[9] S. Dhara, P. Bhargava, Egg white as environmentally friendly low-cost binder for gelcasting of ceramics, Journal of the American Ceramic Society 84 (12) (2001) 3048–3050.
[10] Y. Chen, Z. Xie, J. Yang, Y. Huang, Alumina casting based on gelation of gelatine, Journal of the European Ceramic Society 19 (1999) 271–275.
[11] L.J. Vandeperre, A.M. De Wilde, J. Luyten, Gelatin gelcasting of ceramic components, Journal of Materials Processing Technology 135 (2003) 312–316.
[12] F.S. Ortega, F.A.O. Valenzuela, C.H. Scaracchio, V.C. Pandolfelli, Alternative gelling agents for the gelcasting of ceramic foams, Journal of the European Ceramic Society 23 (2003) 75–80.
[13] J.M. Tulliani, V. Naglieri, M. Lombardi, L. Montanaro, Porous alumina and zirconia bodies obtained by a novel gel casting process, in: R. Narayan, P. Colombo (Eds.), Proceedings of the 32nd International Conference & Exposition on Advanced Ceramics and Composites, Daytona Beach (FL), 2008.
[14] M. Lombardi, L. Montanaro, L. Grémillard, J. Chevalier, New gelcasting procedure to prepare alumina porous components: Process optimization and preliminary mechanical tests, in: R. Narayan, P. Colombo (Eds.), Proceedings of the 32nd International Conference & Exposition on Advanced Ceramics and Composites, Daytona Beach (FL), 2008.
[15] P. Sepulveda, Gelcasting foams for porous ceramics, The American Ceramic Society Bulletin 76 (10) (1997) 61–65.
[16] D.B. Marshall, T. Noma, A.G. Evans, A simple method for determining elastic-modulus-to-hardness ratios using Knoop indentation measurements, Journal of the American Ceramic Society 65 (10) (1982) C175–C176.
[17] D. Tabor, The Hardness of Metals, Clarendon Press, Oxford, 1951.
[18] J. Gong, J. Wu, Z. Guan, Examination of the indentation size effect in low-load Vickers hardness testing of ceramics, Journal of the European Ceramic Society 19 (1999) 2625–2631.
[19] J.C. Glandus, T. Rouxel, Study of the Y-TZP toughness by an indentation method, Ceramics International 17 (1991) 129–135.
[20] J.D. Lin, J.G. Duh, Fracture toughness and hardness of ceria- and yttria-doped tetragonal zirconia ceramics, Materials Chemistry and Physics 78 (2002) 253–261.
[21] G.R. Anstis, b.P. Chantikul, R. Lawn, D.B. Marshall, A critical evaluation of indentation techniques for measuring fracture toughness. I. Direct crack measurements, Journal of the American Ceramic Society 64 (9) (1981) 533–538.
[22] R. Lawn, A.G. Evans, D.B. Marshall, Elastic plastic indentation damage in ceramics: the median/radial crack system, Journal of the American Ceramic Society 63 (9–10) (1980) 574–581.
[23] M.T. Laugier, The elastic/plastic indentation of ceramics, Materials Science Letters 4 (1985) 1539–1541.
[24] K. Niihara, R. Morena, D.P.H. Hasselman, Evaluation of K_{Ic} of brittle solids by the indentation method with low crack-to-indent ratios, Journal of Materials Science Letters 1 (1) (1982) 13–16.
[25] M.T. Laugier, New formula for indentation toughness in ceramics, Journal of Materials Science Letters 6 (1987) 355–356.
[26] J. Lankford, Indentation microfracture in the Palmqvist crack regime: implication for fracture toughness evaluation by the indentation method, Journal of Materials Science Letters 1 (1982) 493–495.
[27] D. Chicot, A. Pertuz, F. Roudet, M.H. Staia, J. Lesage, New developments for fracture toughness determination by Vickers indentation, Materials Science and Technology 20 (7) (2004) 877–884.
[28] W.C. Oliver, G.M. Pharr, Improved technique for determining hardness and elastic modulus using load and displacement sensing indentation experiments, Journal of Materials Research 7 (6) (1992) 1564–1580.
[29] W.C. Oliver, G.M. Pharr, Review: measurement of hardness and elastic modulus by instrumented indentation: advances in understanding and refinements to methodology, Journal of Materials Research 19 (1) (2004) 3–20.
[30] R.B. King, Elastic analysis of some punch problems for a layered medium, International Journal of Solids and Structures 23 (12) (1987) 1657–1664.
[31] O. Sahin, O. Uzun, M. Sopicka-Lizer, H. Gocmez, U. Kölemen, Analysis of load-penetration depth data using Oliver–Pharr and Cheng–Cheng methods of SiAlON–ZrO_2 ceramics, Journal of Physics D: Applied Physics 41 (2008) 1–8.
[32] B.J. Briscoe, S.J. Sinha, Density distributions characteristics of green ceramic compacts using scratch hardness, Tribology International 30 (7) (1997) 475–482.
[33] J. Luo, R. Stevens, Porosity-dependence of elastic moduli and hardness of 3Y-TZP ceramics, Ceramics International 25 (1999) 281–286.
[34] B.Y. Jang, Influence of low indentation load on Young's modulus and hardness of 4 mol.% Y_2O_3–ZrO_2 by nanoindentation, Journal of Alloys and Compounds 426 (2006) 312–315.
[35] J.M. Meza, M.C.M. Farias, R.M. de Souza, L.J.C. Riano, Using the ratio: maximum load over unload stiffness squared, Pm/Su^2, on the evaluation of machine stiffness and area function of blunt indenters on depth-sensing indentation equipment, Materials Research 10 (4) (2007) 437–447.
[36] M. Troyon, L. Huang, Correction factor for contact area in nanoindentation measurements, Journal of Materials Research 20 (3) (2005) 610–617.
[37] Z. Peng, J. Gong, H. Miao, On the description of indentation size effect in hardness testing for ceramics: analysis of the nanoindentation data, Journal of the European Ceramic Society 24 (2004) 2193–2201.
[38] J. Gong, J. Wang, Z. Guan, Indentation toughness of ceramics: a modified approach, Journal of Materials Science 37 (2002) 865–869.
[39] A.K. Gain, H.Y. Song, B.T. Lee, Microstructure and mechanical properties of porous yttria stabilised zirconia ceramic using poly methyl methacrylate powder, Scripta Materialia 54 (2006) 2081–2085.